2D Modeling and Correction of Fan-Beam Scan Geometry in OCT

Min Chen[1(✉)], James C. Gee[1], Jerry L. Prince[2], and Geoffrey K. Aguirre[3]

[1] Department of Radiology, University of Pennsylvania, Philadelphia, PA 19104, USA
minchen1@upenn.edu
[2] Department of ECE, Johns Hopkins University, Baltimore, MD 21218, USA
[3] Department of Neurology, University of Pennsylvania, Philadelphia, PA 19104, USA

Abstract. A-scan acquisitions in OCT images are acquired in a fan-beam pattern, but saved and displayed in a rectangular space. This results in an inaccurate representation of the scan geometry of OCT images, which introduces systematic distortions that can greatly impact shape and morphology based analysis of the retina. Correction of OCT scan geometry has proven to be a challenging task due to a lack of information regarding the true angle of entry of each A-scan through the pupil and the location of the A-scan nodal points. In this work, we present a preliminary model that solves for the OCT scan geometry in a restricted 2D setting. Our approach uses two repeat scans with corresponding landmarks to estimate the necessary parameters to correctly restore the fan-beam geometry of the input B-scans. Our results show accurate estimation of the ground truth geometry from simulated B-scans, and we found qualitatively promising result when the correction was applied to longitudinal B-scans of the same subject. We establish a robust 2D framework that can potentially be expanded for full 3D estimation and correction of OCT scan geometries.

Keywords: Distortion correction · Retina · OCT

1 Introduction

Optical coherence tomography (OCT) imaging has gained widespread popularity in the past decade for the analysis of retinal health and disease in both clinical and research settings. However, a longstanding limitation of OCT imaging is the absence of scan geometry correction to accurately match the image with its physical acquisition space [2,6,9]. A-scan acquisitions in OCT images are acquired in a fan-beam pattern, however they are saved and visualized in a rectangular pattern. This distorts the resulting image in two ways. First, due to the spread of the fan-beam, the arc distance between A-scans increases with the depth in the scan. When represented as a rectangular pattern, this results in structures deeper in the image to appear compressed. Second, the A-scans on

D. Stoyanov et al. (Eds.): COMPAY 2018/OMIA 2018, LNCS 11039, pp. 328–335, 2018.
https://doi.org/10.1007/978-3-030-00949-6_39

the edges of a fan-beam must travel further than the A-scans at the center of the scan. This causes objects in the periphery of the OCT image to be located deeper in the A-scan. When placed in a rectangular pattern, this results in the appearance that objects are curved downwards when moving away from the center of the scan. Figure 1 shows two examples of distortions due to uncorrected scan geometry on a flat object.

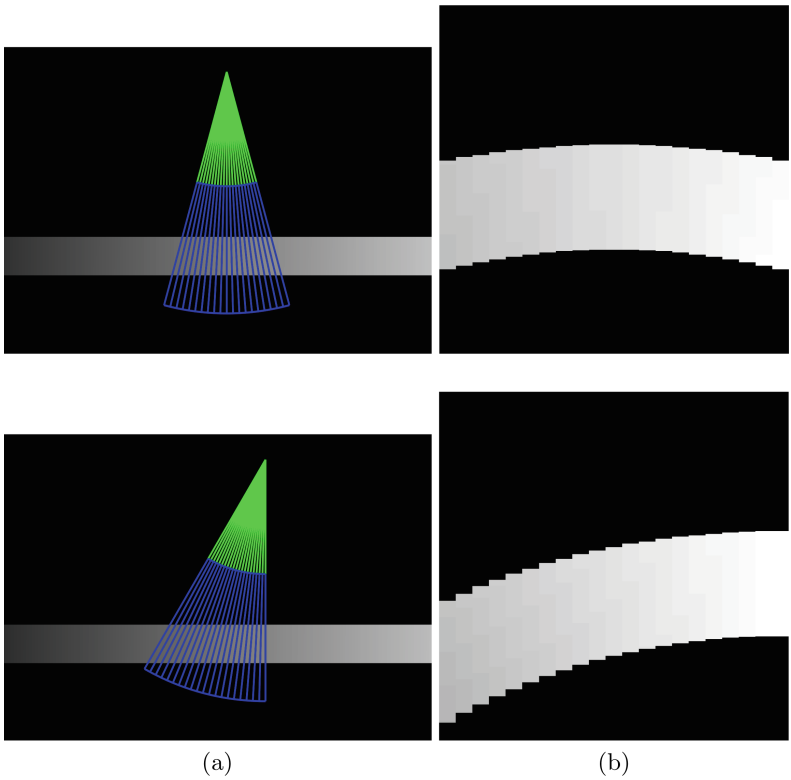

Fig. 1. Two examples of simulated OCT scans and the effect of the scan geometry distortion on a flat object. (a) shows the relative positioning between the fan-beam and the object. Blue represents the scan area acquired in the OCT image, and green is the non-acquired region between the nodal point and OCT image. (b) shows the resulting OCT B-scan of the object, where each column in the image corresponds with a blue A-scan line in the respective image in (a). (Color figure online)

Due to the presence of scan geometry distortions, OCT images do not fully represent the correct underlying physical structure of the retina [6]. However, it is interesting to note that errors from this misrepresentation are largely mitigated in contemporary analysis of OCT which focuses on observing regional means of retinal layer thickness. This is because the thickness of a layer is typically

measured as the direct distance within each A-scan in the OCT [7]. Neither the depth dependent compression of the fan-beam nor the shift of the A-scans in the periphery influences this thickness measure. The main effect that scan geometry has on thickness values is in the non-uniform path each A-scan takes across a layer, resulting in thicker measurements away from the fovea. However this effect is often masked by the natural concentric increase of layer thickness with distance from the fovea, and the use of mean layer thickness for most analysis.

In recent years, addressing the scan geometry of OCT has becomes more important due to the emerging popularity of spatially-based analysis of the shape [5,8] and morphology [1,3,4] of the retina. In contrast to thickness-based analysis, these methods are highly sensitive to structural distortions due to the local specificity of the techniques. However, correcting for the scan geometry of OCT has remained a challenge due to two missing pieces of information that are generally not provided with OCT images: (1) the angle of entry of each A-scan into the pupil and (2) the location of the A-scan nodal point, where the fan-beam is centered. Existing approaches for correcting the scan geometry rely on basic approximations regarding these parameters, such as assuming the beam entry is always centered or approximating the nodal point location using the subject's axial length [6].

In this work we present a 2D model for B-scan OCT acquisitions, which we use to generate simulated images with specific scan geometry distortion. We then present an analytic approach for solving the missing parameters of the model using trigonometric relationships established between corresponding landmarks from two different scans.

2 Method

2.1 OCT Fan-Beam Geometry

We represent the fan-beam geometry of the OCT image as a polar coordinate system where the origin, C, is the nodal point where the A-scans intersect, and (c_x, c_y) is the location of C in the Cartesian (physical) coordinate system. ϕ_n is polar coordinate angle of the nth A-scan in the OCT image. R is the distance from the nodal point to the top of the OCT scan, and r_n is the A-scan measurement from the top of the OCT scan to the surface of the retina. Figure 2 shows a diagram of this model. For a physical location (x_n, y_n) on the surface of the retina, we can describe it in terms of the image coordinate system using standard conversion between polar and Cartesian coordinates:

$$x_n = (R + r_n)\cos(\phi_n) + c_x \tag{1}$$

$$y_n = (R + r_n)\sin(\phi_n) + c_y. \tag{2}$$

2.2 Two Scan Solution

Given the geometry described in Sect. 2.1, we introduce an approach for solving for the length of R and relative location of C when given two scans (with nodal

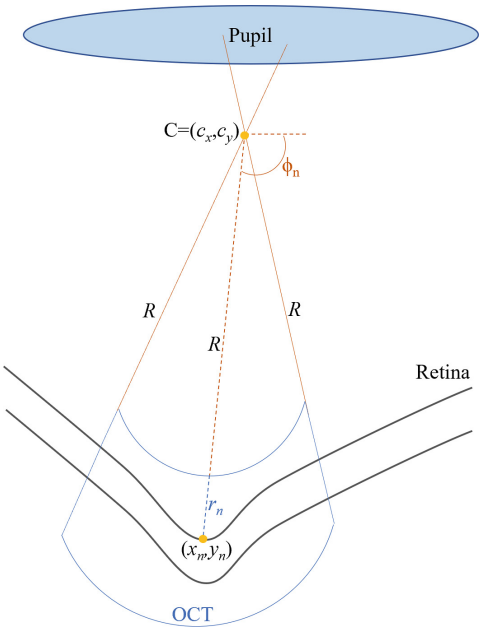

Fig. 2. Diagram of the OCT fan-beam geometry in our model. C is the location of the nodal point, R is a constant distance from C to the beginning of the OCT scan. For the nth A-scan, r_n is the distance from the retina to the beginning of the scan and ϕ_n is the polar angle of the A-scan.

points C_A and C_B) with corresponding landmarks (x_1, y_1) and (x_2, y_2). Figure 3 shows the geometric setup for the problem. We see from the diagram that the nodal points and corresponding landmarks form two triangles with a shared side L. $r_1^A, r_2^A, r_1^B, r_2^B$ are the distance from each A-scan in images A and B to (x_1, y_1) and (x_2, y_2), respectively. $\alpha_{1,2}^A$ and $\alpha_{1,2}^B$ are the angles between the two A-scans associated with the landmarks in each image. These angles can be found as a fraction of the total angular field of view of each scan. Using the law of cosines on both triangles, we can establish the equivalency:

$$L^2 = (R + r_1^A)^2 + (R + r_2^A)^2 - 2(R + r_1^A)(R + r_2^A)\cos(\alpha_{1,2}^A) \tag{3}$$

$$L^2 = (R + r_1^B)^2 + (R + r_2^B)^2 - 2(R + r_1^B)(R + r_2^B)\cos(\alpha_{1,2}^B). \tag{4}$$

This allows us to solve for R as a quadratic equation:

$$R = \frac{-b \pm \sqrt{(b^2 - 4ac)}}{2a} \tag{5}$$

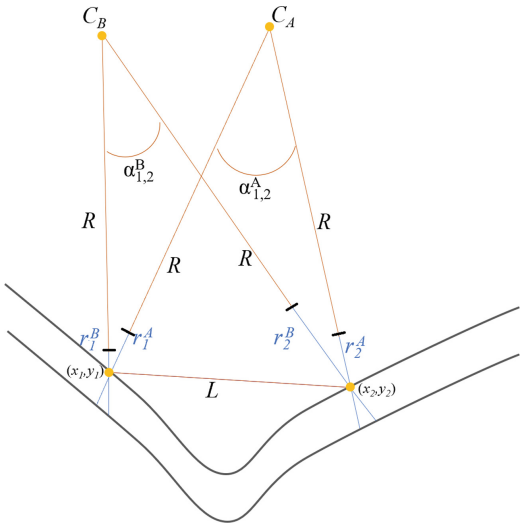

Fig. 3. Diagram of our approach for using two scans to solve for the nodal points C_A and C_B and, R, the constant distance from each OCT scan to its nodal point.

where,

$$a = 2(\cos(\alpha^A_{1,2}) - \cos(\alpha^B_{1,2})) \tag{6}$$

$$b = 2(r^B_1 r^B_2(1 - \cos(\alpha^B_{1,2})) - r^A_1 r^A_2(1 - \cos(\alpha^A_{1,2}))) \tag{7}$$

$$c = (r^B_1)^2 + (r^B_2)^2 - (r^A_1)^2 + (r^A_2)^2 - 2(r^B_1 r^B_2 \cos(\alpha^B_{1,2}) - r^A_1 r^A_2 \cos(\alpha^A_{1,2})). \tag{8}$$

Taking the positive solution for R, we can then use Eqs. 1 and 2 to place each A-scan from each image into the physical coordinate space. This is done by first setting the nodal point as the origin $(c_x, c_y) = (0, 0)$ and placing the first A-scan at zero degrees ($\phi_1 = 0$). This allows both images to be converted from their polar coordinate systems into Cartesian coordinate systems. Once in Cartesian space, we can then apply a rigid body rotation and translation such that the thinnest line that crosses the fovea center is aligned with the visual axis of the eye (see Fig. 5b).

3 Evaluation and Results

3.1 Simulated Reconstruction

One challenge in modeling and correcting for the scan geometry in retinal OCT is the lack of a ground truth representation for the retina being imaged. Thus, it is difficult to assess if the scan geometry was accurately corrected. To evaluate our approach, we use our model to generate simulated OCT images from specific scan geometries (see Fig. 1a). Each voxel of the object in the simulation is tagged

with a unique identifier, which can be observed as the gradient in Fig. 1a. Using these identifier, this allows us to establish voxel-wise correspondences between two simulated OCT images.

Our correction method was applied to these simulated OCT images using two randomly chosen locations in the images as landmarks to estimate R. This process was repeated 10000 times to acquire a distribution of the R estimated from the simulated OCT images. Figure 4 shows a histogram of the estimated R from the 10000 trials. From the figure we see that majority of the estimated R were clustered around the true distance of $R = 500$ pixels. There were however several degenerate estimations of zero and infinity for R which resulted when the two randomly chosen landmarks were too close together or co-linear, causing the equation to have zero or infinite solutions. Ignoring these degenerate cases, the RMSE of the estimated R compared to the ground truth in this experiment was 84.9 pixels, which is a mean spread of 16.98% relative to the ground truth R length being estimated.

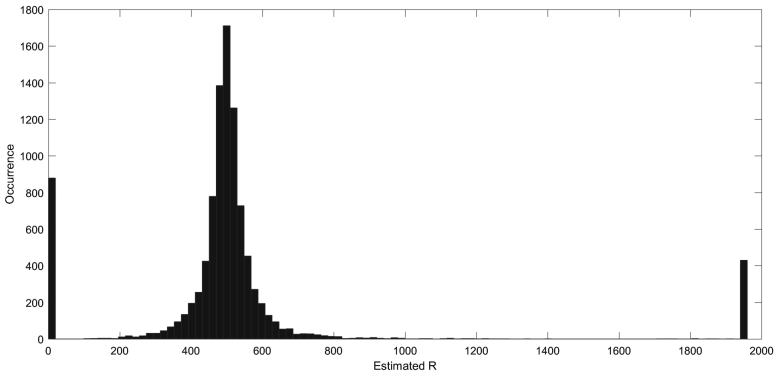

Fig. 4. Histogram of the estimated R across 10000 random trials using simulated OCT images with a ground truth $R = 500$.

3.2 Application to Real Data

We also applied our approach for correcting the scan geometry of real OCT data. A corresponding pair of B-scans from longitudinal OCT scans of the same subject was manually selected. A pair of vessel locations in each B-scan was then selected and used as corresponding landmarks, and our approach was applied to the images to correct for the scan geometry in both images simultaneously. Both corrected images were then realigned such that the fovea is centered. Figure 5 shows the original and corrected images. Since the true distortion and the shape of the underlying retina is unknown, this primarily served as a preliminary demonstration of our technique on real data. Qualitatively, we observe that the shape and structure of the retina became better aligned after correcting for the scan geometry. However, unlike an image registration technique where one image is used as a reference and the other image is transformed to match, our

approach solves and corrects for the underlying shared geometry of the retina in both images. Thus, our approach increased the similarity between the images without being biased towards a chosen reference.

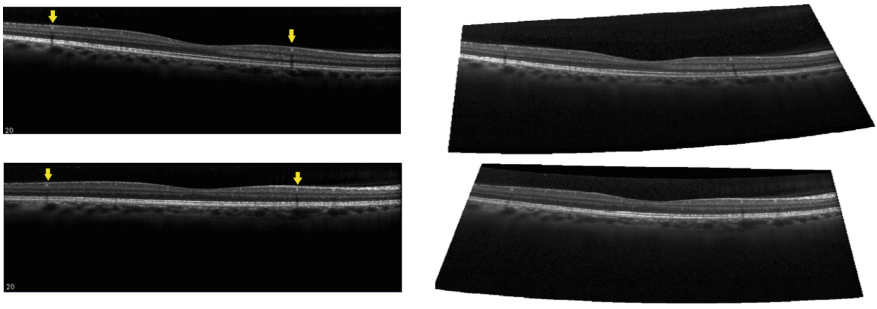

(a) (b)

Fig. 5. Example of the proposed scan correction on a pair of longitudinal B-scans from the same subject. Yellow arrows indicate the two pairs of vessel locations used as corresponding landmarks for our method. (a) shows the two original B-scan images. (b) shows the resulting images after correcting for the scan geometry. (Color figure online)

4 Discussion

4.1 Simulation Errors

From Fig. 4 we see that even for a simulated reconstruction of the scan geometry, there is still a distribution of error when estimating R. The primary source of this error comes from the discretization of the object as it is converted into the simulated B-scans. Since the corresponding landmarks are establish as pairwise voxels, the precise location of a corresponding feature can be lost due to the voxel resolution. This error then translates to inaccuracies in the reconstruction of the scan geometry.

4.2 Limitations

We observe two primary limitations to our proposed approach. First, the 2D model currently limits the practicality of the method for use with real 3D OCT images. While in Sect. 3.2 we were able to find two corresponding B-scans to apply our method, often corresponding landmark locations between OCT images will not necessary land on the same B-scan. To address this, we are currently working to extend the model to a 3D solution, which will account for the scan geometry along both the A-scan and B-scan directions. Second, we recognize that a repeat scan of the same subject may not always be available to be used with our approach. Thus we are looking into adaptations of this method that will be able to use different types of regularly acquired scans (e.g. horizontal and vertical scans) to reduce this limitation.

5 Conclusion

In this work we introduced a 2D model for correcting the fan-beam geometry of OCT B-scans. From the model, we derived an analytic solution for solving the unknown location and distance of the nodal point from a pair of B-scans, which showed promising results in simulated and real data. Our goal is to establish a robust 2D framework that will be expanded in the future for full 3D estimation and correction of OCT scan geometries. This correction will allow for more accurate analysis of retinal shape and morphology for the study of retinal health and disease.

Acknowledgment. This work was supported by our funding sources NEI/NIH grants P30EY001583, 1R01EY024655 and U01EY025864.

References

1. Antony, B.J., et al.: Voxel based morphometry in optical coherence tomography: validation and core findings. In: Medical Imaging 2016: Biomedical Applications in Molecular, Structural, and Functional Imaging, vol. 9788, p. 97880P. International Society for Optics and Photonics (2016)
2. Asami, T., et al.: Development of a fiber-optic optical coherence tomography probe for intraocular use. Investig. Ophthalmol. Vis. Sci. **57**(9), OCT568–OCT574 (2016)
3. Brar, M., et al.: Correlation between morphological features on spectral domain optical coherence tomography and angiographic leakage patterns in macular edema. Retina (Philadelphia, Pa.) **30**(3), 383 (2010)
4. Chen, M., Lang, A., Ying, H.S., Calabresi, P.A., Prince, J.L., Carass, A.: Analysis of macular oct images using deformable registration. Biomed. Opt. Express **5**(7), 2196–2214 (2014)
5. Kajić, V., et al.: Robust segmentation of intraretinal layers in the normal human fovea using a novel statistical model based on texture and shape analysis. Opt. Express **18**(14), 14730–14744 (2010)
6. Podoleanu, A., Charalambous, I., Plesea, L., Dogariu, A., Rosen, R.: Correction of distortions in optical coherence tomography imaging of the eye. Phys. Med. Biol. **49**(7), 1277 (2004)
7. Schuman, J.S., et al.: Reproducibility of nerve fiber layer thickness measurements using optical coherence tomography. Ophthalmology **103**(11), 1889–1898 (1996)
8. Sibony, P., Kupersmith, M.J., Rohlf, F.J.: Shape analysis of the peripapillary rpe layer in papilledema and ischemic optic neuropathy. Investig. Ophthalmol. Vis. Sci. **52**(11), 7987–7995 (2011)
9. Westphal, V., Rollins, A.M., Radhakrishnan, S., Izatt, J.A.: Correction of geometric and refractive image distortions in optical coherence tomography applying fermat's principle. Opt. Express **10**(9), 397–404 (2002)